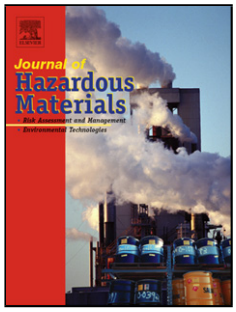

Title: Microbubble enhanced ozonation process for advanced treatment of wastewater produced in acrylic fiber manufacturing industry

Author: Tianlong Zheng Qunhui Wang Tao Zhang Zhining Shi Yanli Tian Shanshan Shi Nicholas Smale Juan Wang

PII: S0304-3894(15)00080-1
DOI: http://dx.doi.org/doi:10.1016/j.jhazmat.2015.01.069
Reference: HAZMAT 16570

To appear in: *Journal of Hazardous Materials*

Received date: 27-12-2014
Revised date: 28-1-2015
Accepted date: 30-1-2015

Please cite this article as: Tianlong Zheng, Qunhui Wang, Tao Zhang, Zhining Shi, Yanli Tian, Shanshan Shi, Nicholas Smale, Juan Wang, Microbubble enhanced ozonation process for advanced treatment of wastewater produced in acrylic fiber manufacturing industry, Journal of Hazardous Materials http://dx.doi.org/10.1016/j.jhazmat.2015.01.069

Microbubble Enhanced Ozonation Process for Advanced Treatment of Wastewater Produced in Acrylic Fiber Manufacturing Industry

Tianlong Zheng[1], Qunhui Wang[1,2,*], Tao Zhang[3], Zhining Shi[4], Yanli Tian[1], Shanshan Shi[1], Nicholas Smale[4], Juan Wang[1]

1. Department of Environmental Engineering, University of Science and Technology Beijing, 30 Xueyuan Road, Haidian District, Beijing 100083, China;

2. Beijing Key Laboratory on Resource-oriented Treatment of Industrial Pollutants, University of Science and Technology Beijing, 30 Xueyuan Road, Haidian District, Beijing 100083, China;

3. Water Desalination and Reuse Center, King Abdullah University of Science and Technology, Thuwal 4700, Kingdom of Saudi Arabia;

4. School of Earth and Environmental Sciences, The University of Adelaide, South Australia 5005, Australia.

Contact information of authors:

1. Tianlong Zheng. Tel. / Fax: +86 010 62332778, Email: skytal_03@sina.com;

2. Qunhui Wang. Tel. /Fax: +86 010 62332778, Email: wangqh59@sina.com;

3. Tao Zhang. Tel. /Fax: +966 (0) 2 808 4920, Email: tao.zhang@kaust.edu.sa;

4. Zhining Shi. Tel. /Fax: +86 010 62332778, Email: zhining.shi.career@gmail.com;

5. Yanli Tian. Tel. /Fax: +86 010 62332778, Email: tianli5921@126.com;

6. Shanshan Shi. Tel. /Fax: +86 010 62332778, Email: shishanshan727@gmail.com;

7. Nicholas Smale. Tel. /Fax: +61 03 96677527, Email: NSmale@bionicsinstitute.org;

8. Juan Wang. Tel. /Fax: +86 010 62332778, Email: pizi0909@163.com;

Highlights

1. Characterisation of wet spun acrylic fiber manufacturing industry wastewater.

2. Microbubble-ozonation of acrylic fiber industry wastewater.

3. Improved organic removal and biodegradability by microbubble ozonation.

Abstract

This work investigated microbubble-ozonation for the treatment of a refractory wet-spun acrylic fiber wastewater in comparison to macrobubble-ozonation. COD_{cr}, NH_3-N, and UV_{254} of the wastewater were removed by 42%, 21%, and 42% respectively in the microbubble-ozonation, being 25%, 9%, and 35% higher than the removal rates achieved by macrobubble-ozonation at the same ozone dose. The microbubbles (with average diameter of 45 μm) had a high concentration of 3.9×10^5 counts/mL at a gas flow rate of 0.5 L/min. The gas holdup, total ozone mass-transfer coefficient, and average ozone utilization efficiency in the microbubble-ozonation were 6.6, 2.2, and 1.5 times higher than those of the macrobubble-ozonation. Greater generation of hydroxyl radicals and a higher zeta potential of the bubbles were also observed in the microbubble ozonation process. The biodegradability of the wastewater was also significantly improved by microbubble-ozonation, which was ascribed to the enhanced degradation of alkanes, aromatic compounds, and the many other bio-refractory organic compounds in the wastewater. Microbubble-ozonation can thus be a more effective treatment process than traditional macrobubble-ozonation for refractory wastewater produced by the acrylic fiber manufacturing industry.

Keywords: acrylic fiber manufacturing wastewater; advanced treatment; microbubble-ozonation; macrobubble-ozonation

1. Introduction

Driven by increasing demand, acrylic fiber which is widely used in the production of blankets, artificial fur, and plush toys, has achieved a rapid increase in production since its industrialization in the 1950s. The annual production of acrylic fibers is nearly 0.7 million tons, which is associated with the discharge of more than 9.35 million tons of wastewater that contains 13.6 thousand tons of chemical oxygen demand (COD). The wastewater discharged from the acrylic fiber manufacturing industry comprises of a significant amount of refractory organics and inorganics such as nitriles, phenols, benzene, ester, SCN^- and their oligomers. Biodegradation is not efficient for the treatment of this kind of wastewater due to the poor biodegradability of less than 0.02.

Presently, techniques for acrylic fiber wastewater treatment mainly include membrane filtration, adsorption, coagulation, internal electrolysis and biological treatment with sequence bioreactor (SBR), biofilter, or biological

contact oxidation tower. Even with use of these technologies it is still difficult to achieve effluent qualities that satisfy discharge standards. Because various physical and chemical pretreatment techniques cause only limited improvement to the biodegradability of such wastewater, biological treatment combined with advanced oxidation [1] is one of the most promising treatment processes. Ozone has a high oxidation potential and has been widely used for disinfection and the removal of organics for water and wastewater treatment [2-4]. The present ozonation treatment process is limited by low ozone dissolution and a slow mass transfer rate, leading to low utilization efficiency of gaseous ozone and thus high operation costs [5]. Efficient techniques for ozone transfer are especially desired for the treatment of wastewater containing high concentrations of organic pollutants.

Microbubble wastewater treatment has drawn great attention for its small bubble size (less than 50 μm), huge interfacial area, long stagnation time, lower bubble rising speed, and high interior pressure [6]. The microbubble technology has been widely used in many fields of application, especially in environmental engineering [7], biomedical engineering [8], and other industrial productions [9]. Regarding microbubble ozonation, research has focused not only on the properties of microbubbles (e.g., zeta potential) but also on the improvement of oxidative removal of pollutants [10, 11]. To date, there are few studies on the application of microbubble-ozonation for acrylic fiber wastewater treatment.

In this study, microbubble-ozonation and macrobubble-ozonation were compared for the treatment of wastewater that had been discharged from a wet-spun acrylic fiber manufacturing plant. The efficiency in terms of COD_{cr}, UV_{254}, and NH_3-N removal as well as the improvement in biodegradability was investigated. The bubbles produced in the two processes were also compared in terms of gas holdup, ozone mass transfer coefficient, ozone utilization efficiency, hydroxyl radical production, and zeta potential to explain the differences of the two processes for the treatment of the acrylic fiber wastewater.

2. Experimental

2.1. Wastewater

The experimental wastewater was secondary effluent of an acrylic fiber manufacturing plant in Northern China. The wastewater was stored at 4 °C before use. The physical and chemical properties of the wastewater are shown in Table 1. This wastewater is characteristic in its complicated components, high toxicity, and low biodegradability.

Table 1 Characteristics of the acrylic fiber wastewater.

2.2. Experimental setup and procedure

The experimental apparatus is shown in Fig. 1. The reactor was made of transparent rigid Plexiglas with an inner diameter of 80 mm, height of 1200 mm, and effective volume of 6 L. A TCRI microbubble generator (Japan) was used to produce microbubbles with a mean bubble size less than 45 μm under the operation pressure of 0.4 MPa. A 40 μm cylindrical micropore titanium plate placed at the bottom of the reactor was used to generate macrobubbles (mean bubble size of about 1 mm) from the ozone gas for comparison. Ozone gas was produced at 5 g/h with an ozone generator (CF-YG5, Shanmei Shuimei Co. Beijing) using dried air as gas source.

Fig. 1. Schematic diagram of the experimental setup.

At the beginning of the experiment, 3 L of acrylic fiber wastewater was pumped into the reactor with a peristaltic pump. When conducting microbubble ozonation, the macrobubble pathway was closed, and vice versa. In microbubble ozonation, the wastewater was continuously circulated between the microbubble generator and the reactor.

Ozone gas exhausted from the reactor was absorbed with 2% KI solution. The temperature of the reaction solution was maintained at 20 ^{o}C throughout the treatment. Samples were taken at predetermined time intervals. Any residual ozone in the sample was immediately purged with nitrogen gas.

2.3. Analytical methods

Most of the wastewater quality parameters were measured according to *The Water and Wastewater Monitoring and Analysis Method (4th Edition)* [12]. In addition, COD_{cr}, BOD_5, TOC, and UV_{254} were respectively measured by a COD rapid digestion apparatus (DIS-1A, Shenzhen Changhong Instru. CO., LTD, China), oxiTop system (OxiTop, WTW, Germany), vario TOC analyzer (vario TOC, Elementar, Germany) and a UV-visible spectrophotometer (UV-752, METASH, China). The dissolved oxygen concentration and the pH were determined with a dissolved oxygen meter (HQ30D, Hach, USA) and

automatic potentiometric titrator meter (ZD-2, LEICI, China) respectively at 20 ºC. The gaseous ozone concentration was mesasured with the iodometric method [13]. The concentration of dissolved ozone was tested with the indigo colorimetric method (Standard Method 4500-O_3 B) [14].

The size of the microbubbles was measured with a microscope (Nikon, YS100, Nikon Corporation Instrument Company, Japan) equipped with a digital camera. The zeta potential of the surface of ozone microbubbles in the water was averaged over ten measurements with a zeta potential analyzer (DB-525, Brookhaven, USA).

The determination of gas holdup was measured with a volume expansion method [15]. The Equation was as follows:

$$\varepsilon_g = (1-\frac{V_0}{V})\times 100\% = (1-\frac{H_0}{H})\times 100\% \quad (1)$$

where ε_g is gas holdup, V_0 is valid water volume before aeration, V is valid water volume after aeration, H_0 is valid water height before aeration, H is valid water height after aeration. Since the cross sectional area is the same, the variation of water height could represent that of the water volume.

2.4. Three-dimensional excitation-emission matrix (3D-EEM) fluorescence spectroscopy

The hydroxyl radical concentration was tested qualitatively with a three-dimensional excitation-emission matrix fluorescence spectroscopy (3D-EEM) (F2700, Hitachi, Japan) after reaction with disodium salt of terephthalic acid (NaTA) and filtration with a 0.45 μm PVDF membrane. NaTA reacts with hydroxyl radicals to form 2-hydroxyterephthalic acid (HTA) that gives a bright stable fluorescence ($\lambda_{emission}$ = 425 nm, $\lambda_{excitation}$ = 315 nm) [16]. TA and NaTA are extensively applied to detect hydroxyl radicals produced in aqueous phase [17, 18]. In this study, air and ozone micro/macro-bubble water (5 mL) were reacted with 0.5 mM NaTA (5 mL) at the pH of 6.85 in which the buffer was 10 mM mixed non-fluorescent phosphate solution. The samples were analyzed within a few hours of being collected. EEM spectra were taken at a scanning speed of 1500 nm/min, while the slit width for excitation (varied from 200 to 450 nm) and emission beams (varied from 280 to 500 nm) was 10 and 2 nm, respectively.

2.5. GC/MS measurement

Gas chromatography/mass spectrometry (GC/MS) was used for the analysis of the main organic compounds in the wastewater. For GC/MS analysis, the wastewater sample (150 mL) was extracted with 50 mL of CH_2Cl_2 (Chromatogram Pure Grade, Fisher) three times under acidic (pH 2.0), neutral (pH 7.0) and alkaline (pH 12.0) conditions, respectively. The three extracts were mixed together,

dehydrated with anhydrous sodium sulfate and dried under the flow of nitrogen gas. The residual was dissolved in 1.0 mL of CH_2Cl_2 and then injected into a Shimadzu GCMS-QP2010plus system (Shimadzu., Japan) at the volume of 1 μL. The column used was a 30 m × 0.25 mm i.d., J&W Scientific 122-5032 DB-5 (5% diphenyl-dimethylpolysiloxane; USA) capillary column with a film thickness of 0.25 μm. The GC oven temperature was maintained at 50 °C for 1 min, raised at a rate of 10 °C min^{-1} to 60 °C (held for 2 min), and then further raised at 10 °C min^{-1} to 250 °C (held for 5 min). The MS ion source temperature was 300 °C and electron energy was 70 eV. Identification of the compounds was based on the NIST 05 mass spectral library database.

3. Results and Discussion

3.1. The effectiveness of microbubble-ozonation and macrobubble-ozonation

Compared with macrobubble-ozonation, the microbubble-ozonation produced milky microbubbles with relatively small size and long retention time in the reactor. Fig. 2 shows the reduction of COD_{cr}, NH_3-N, and UV_{254} and the variation of BOD_5/COD_{cr} over time for the wastewater during microbubble-ozonation and macrobubble-ozonation.

Fig. 2. The variation of a) COD_{cr}, b) NH_3-N, c) UV_{254}, and d) BOD_5/COD_{cr} with time (solid symbols: microbubble-ozonation; open symbols: macrobubble-ozonation). Error bars represent standard deviation of three replicates.

The maximum removal rates of COD_{cr}, NH_3-N, and UV_{254} by the microbubble-ozonation were 42%, 21%, and 42%, respectively, which were 25%, 9%, and 35% higher than those achieved by the macrobubble-ozonation. The BOD_5/COD_{cr} of wastewater treated with microbubble-ozonation and macrobubble-ozonation was improved from 0.04 to 0.13 and 0.08, i.e., 3.3 and 2.0 times respectively higher than that of the raw wastewater.

The COD_{cr} increased after reaction for 45 min, especially in the microbubble-ozonation condition (Fig. 2a). According to the literature [19], that refractory organic matter which cannot be detected with COD measurement (the COD could not be oxidized by $K_2Cr_2O_7$) can be degraded by hydroxyl radicals into organics detectable with COD measurement. Therefore, this increase in COD_{cr} is probably due to oxidation of some refractory organics by hydroxyl radicals during ozonation. The removal of ammonia was insignificant in the two processes. A slight improvement in the removal rate was observed in microbubble-ozonation compared to macrobubble-ozonation. This is possibly due to more hydroxyl radicals being produced in the

former, because ozone itself is relatively unreactive towards free NH_3. The reaction rate constants for ozone and hydroxyl radicals with free NH_3 are 2.0×10^2 $M^{-1}s^{-1}$ and 8.7×10^7 $M^{-1}s^{-1}$, respectively [20]. UV_{254} removal was quite different between the two processes (Fig. 2c). UV_{254} decreased from 0.40 to 0.25 in microbubble-ozonation, while in macrobubble-ozonation it increased first to 0.51 in 45 min and then gradually decreased to 0.38. Microbubble-ozonation performed better in the degradation of UV_{254} because of its superior oxidation mechanism, which was also found in the treatment of coke wastewater [11] and dye wastewater [21]. The biodegradability of the two processes gradually increased with reaction time (Fig. 2d).

This wastewater has a high content of refractory organics, such as alkanes, aromatic, phenols, nitriles, amides, and esters. Compared with macrobubble-ozonation, microbubble-ozonation possessed a much greater dissolved ozone concentration and a higher ozone utilization rate in this study. Microbubble-ozonation could also produce more hydroxyl radicals because of a higher ozone mass transfer coefficient. Furthermore, the collapse of microbubbles could also generate hydroxyl radicals, which is related to ionic accumulation around the collapsing micro-bubbles [22]. Therefore, microbubble-ozonation process had high dissolved ozone concentration and hydroxyl radical production. In contrast, less hydroxyl radical generation and dissolved ozone concentration in the macrobubble-ozonation process resulted in a lower extent of oxidation of the refractory organics and consequently a lower biodegradability of the treated wastewater.

3.2. The mechanism of enhanced ozonation process by microbubbles.

3.2.1. Ozone gas holdup

Research has found that gas holdup depends mainly upon gas flow rate, bubble size, and the type of water [23, 24]. In this experiment, the gas flow rate in the two ozonation processes was fixed at 0.5 L/min. The average bubble size was 45 μm and 1 mm in microbubble and macrobubble ozonation, respectively. Fig. 3 shows the variation of gas holdup with time and dissolved ozone concentration.

Fig. 3. Gas holdup in deionized water during aeration with microbubble and macrobubble (solid symbols: microbubble-ozonation; open symbols: macrobubble-ozonation). Error bars represent standard deviation of three replicates.

The gas holdup of ozone microbubbles rapidly increased to saturation (15.1%) within 7 min. In contrast, the saturated gas hold up of ozone macrobubble was only 2.3%, 6.6 times lower than the microbubble ozonation. In addition, the gas holdup of these two kinds of bubbles increased with

dissolved ozone concentration (Fig. 3b). More interestingly, the gas holdup of ozone microbubbles was much higher than that of ozone macrobubbles under the same dissolved ozone concentration, and that the difference between these two bubbles in gas holdup increased with dissolved ozone concentration. This could be attributed to higher dissolution ability and a longer retention time of microbubbles in the water.

The internal pressure of the bubbles, which had a great effect on the dissolution, was largely related to bubble size. The Young–Laplace equation can be applied to calculate the internal pressure of the bubble [25].

$$P_g = P_l + \frac{4\sigma}{d_b} \quad (2)$$

where P_g is the interior gas pressure of the bubble (Pa); P_l is the exterior liquid pressure of the bubble (Pa); σ is the surface tension of the bubble ($N.m^{-1}$), and d_b is the diameter of the bubble (m). According to the Young-Laplace equation (Eq. (2)), the internal pressure of a 1 μm bubble is 3.85 times than that of 1 mm bubble [26]. According to the Henry's Law, high internal pressure of the bubble results in improved dissolution in water [25]. In addition, the concentrations of microbubbles and macrobubbles, with average diameters of 45 μm and 1 mm respectively, were calculated to be 3.9×10^5 and 5.5 counts/mL, respectively. Therefore, the fact that gas holdup of ozone microbubbles was higher than that of macrobubbles can be ascribed to its higher dissolution capacity in the water.

According to the Stokes' law, the rising speed of bubbles which determines their retention time in the water is mainly related to the bubble size [27]. In the current study, the Stokes' law was applied to roughly calculate the rising velocity of bubbles,

$$V = \frac{1}{18} \times \frac{gd^2}{v} \quad (3)$$

where V is the rising velocity of the bubble (m/s), g is the gravitational acceleration (m/s^2), d is the diameter of the bubble (m), and υ is the kinematic viscosity of water (m^2/s). The average sizes of microbubbles and macrobubbles were 45 μm and 1 mm, respectively. Their rising velocities were approximately 0.82 and 240 mm/s, respectively. The effective height of the reactor was 600 mm. So, the retention time of microbubble and macrobubble were 730 and 2.5 s, respectively. The retention time of the former was much greater than that of the later, which can explain why the difference between these two ozonation processes in gas holdup significantly increased with dissolved ozone concentration. Therefore, the smaller in size the bubble is, the higher gas holdup and longer retention time it will have

in water.

3.2.2. Ozone mass transfer coefficient

The dissolution of ozone gas into water is well known to be a limiting step for ozonation [10]. Ozone transferred into water during the two ozonation processes were compared under the same ozone gas flow rate (0.5 L/min).

Fig. 4. Dissolved ozone concentration (a) and ozone mass transfer coefficient (b) in deionized water of the two ozonation processes (solid symbols: microbubble-ozonation; open symbols: macrobubble-ozonation). Error bars in Fig. 4a represent standard deviation of three replicates.

Fig. 4a shows that the saturated dissolved ozone concentration of microbubble-ozonation and macrobubble-ozonation was 9.6 and 8.4 mg/L, respectively. Further, the time used to reach saturated dissolved ozone concentration of microbubble-ozonation is only 7 min, which was only half of the latter. Compared with macrobubbles, the microbubbles, owing to small bubble size, good stability and large interfacial area, could efficiently improve the ozone mass transfer coefficient.

In addition, the mass transfer coefficient of ozone was investigated. In general, the variation of dissolved ozone concentration in clean water during aeration follows a first-order kinetic model, which can be expressed as follows:

$$\frac{dC}{dt} = k_L a_t (C_s - C_t) \qquad (4)$$

where k_L is bulk liquid film transfer rate coefficient (m/min), a_t (m^{-1}) donates total specific surface area (A_t/V, A_t is total surface area for transfer (m^2), and V is the volume of water (m^3)), C_S is steady-state ozone concentration during aeration (mg/L), and C_t is the actual ozone concentration in the water body (mg/L) [28].

We assumed that the total volumetric ozone mass-transfer coefficient $k_L a_t$ (min^{-1}) and C_S values remained constant throughout the test. Equation (4) can be integrated to express $ln(C_s - C_t)$ as a function of time t:

$$ln(C_s - C_t) = -k_L a_t \cdot t + C \qquad (5)$$

According to equation (4), the variation of dissolved ozone concentration C_t with time was calculated. Then, the ozone mass transfer coefficient of microbubble and macrobubble-ozonation during the aeration phase were integrated. The results are shown in Fig. 4b. There was a good linear relationship between $ln(C_s - C_t)$ and time. The $k_L a_t$ of microbubble-ozonation and

macrobubble-ozonation was calculated to be 0.3767 min^{-1} and 0.1732 min^{-1}, respectively. The total mass-transfer coefficient of the former was 2.2 times higher than that of the latter. Therefore, compared with macrobubble generator, there is a stronger ozone mass transfer coefficient and higher dissolved ozone concentrations in the microbubble generator. This result was consistent with the literatures about improvement of ozone transfer by microbubble generator. For example, Chu et al [10] found that the microbubble ozone mass transfer coefficient is 1.8 times higher than that of the conventional process, when the mean diameter and interfacial area of the microbubbles are less than 58 μm and more than 334 m^2/m^3, respectively. Liu et al [29] also found that the total ozone mass-transfer coefficient in the microbubble generator (producing bubbles less than 50 μm) is 1.5 times higher than that in the conventional ozonation process.

3.2.3. Ozone utilization efficiency

Fig. 5 shows ozone utilization efficiency when the inlet of ozone gas concentration and the flow rate were 12 mg/L and 0.5 L/min, respectively. The ozone utilization efficiency was calculated with the following equation:

$$\text{Ozone utilization efficiency} = \frac{\text{input ozone concentration} - \text{off-gas concentration}}{\text{input ozone concentration}} \times 100\% \quad (7)$$

Fig. 5. Ozone utilization efficiency and off-gas ozone concentration in the two ozonation processes (circle symbols: ozone utilization efficiency, triangle symbols: off-gas concentration, solid symbols: microbubble-ozonation, and open symbols: macrobubble-ozonation).

The ozone utilization efficiency of microbubble-ozonation was more than 99% during the first 15min; however, the ozone utilization efficiency of macrobubble-ozonation was only 80%. The ozone utilization efficiency of microbubble-ozonation always remained above 85%. In contrast, the ozone utilization efficiency of macrobubble-ozonation significantly decreased to 45% at 120 min. The average ozone utilization efficiency of the former was 1.5 times of the latter. This conclusion is consistent with previous researchers [29, 30]. In addition, the off-gas concentration of microbubble-ozonation absorbed by the tail gas treatment was 0.90 ± 0.45 mg/L, which was just one fifth of macrobubble-ozonation (4.42 ± 2.66 mg/L). Considering the high removal efficiency of contaminants in the microbubble system as described above, we can conclude that microbubble could enhance the ozone mass transfer. This result is similar to that derived by Chu et al., [5] although he studied the mass transfer based on air instead of gaseous ozone. The lower off-gas concentration is

desirable to reduce wastewater treatment costs. Furthermore, because the ozone utilization efficiency decreased with time, intermittent aeration could be adopted to reduce power consumption in practical application.

3.2.4. Hydroxyl radicals

Many researchers have reported that hydroxyl radical generation from ozone was improved when the microbubble collapsed under water. A great amount of chemical energy is released in a few microseconds due to the accumulation of high concentrations of ions on the gas–liquid interface of the collapsing microbubble, which causes the generation of hydroxyl radicals under high temperature and pressure [22]. Takahashi et al. [22] and Li et al. [26] tested the generation of hydroxyl radicals from collapsing micro-bubbles by electron spin-resonance (ESR). Chu et al. [10] proved that the existence of hydroxyl radicals in ozone microbubble water with fluorescence detection. In order to explain the enhancement of oxidation ability of ozone by microbubbles, the hydroxyl radical generation in air-microbubble water, air-macrobubble water, ozone-microbubble water and ozone-macrobubble water was semi-quantitatively measured with 3D-EEM.

Fig. 6. The fluorescence intensity of 2-hydroxyterephthalic acid (HTA) produced through the reaction of hydroxyl radicals with terephthalic acid (NaTA) in a) air- microbubble water, b) air-macrobubble water, c) ozone-microbubble water, and d) ozone-macrobubble water.

Fig. 6 shows that the fluorescence signal of HTA was observed in air-microbubble water but not in air-macrobubble water, which once again supported the conclusion of Takahashi et al [22] and Li et al [26]. Compared with macrobubble-ozonation, the fluorescence intensity of the samples in ozone microbubble water was significantly higher than that in ozone macrobubble water, indicating a greater amount of hydroxyl radicals generated during microbubble-ozonation. The increased hydroxyl radicals in microbubble-ozonation can enhance the oxidation capacity for removal of contaminants. Chu et al. [5] reported that microbubble-ozonation can improve the oxidation of actual textile wastewater which was also ascribed to the production of hydroxyl radicals during the microbubble-ozonation. Khuntia et al. [31] also reported that the ozone microbubbles could effectively oxidize ammonia with the contribution of hydroxyl radicals in the oxidation process.

3.2.5. Zeta potential

The zeta potential of the bubbles played an important role in the attachment and oxidation of

organics and the bubble coalescence, which will affect the chemical and physical characteristics of microbubbles including gas holdup, mass transfer coefficient, and gas utilization efficiency. The pH in aqueous solutions also influences the zeta potential of microbubbles. The results of previous researchers [11, 27] revealed that zeta potential of microbubbles of ozone is negative over a wide range of pH conditions [32]. In general, the bubbles' zeta potentials are positive in the highly acidic solutions. Because the pH varied significantly during the acrylic fiber wastewater treatment (Fig. 7a), the zeta potential of the microbubbles was investigated in neutral and subalkalic deionized water.

Fig. 7. pH variation with time during wastewater (a) and zeta potential of ozone microbubbles in deionized water at neutral and subalkalic condition (b) (solid symbols: microbubble-ozonation; open symbols: macrobubble-ozonation). Error bars in Fig. 7b represent standard deviation of three replicates.

The zeta potential of ozone microbubbles was approximately -33 mV when the pH was 8.0 and still above -20 mV when the pH was reduced to 7.0 (Fig. 7b). The zeta potential of macrobubbles was not measured here because the analyzer was only able to make measurements of bubbles in the range of 20 nm to 100 μm. However, according to the literature [33], the zeta potential becomes more negative with decreasing bubble size in distilled water. The ozone microbubble possibly had a higher zeta potential than that of the macrobubbles, which could reduce the coalescence of the bubbles and extend retention time of the bubbles in water.

3.3. Enhancement in the degradation of organics

Fig. 8a shows that more than 25 organic compounds were identified in the raw wastewater (summarized in Table 2). These compounds mainly include 14 alkanes (accounting for 69.7% total peak area) and 5 aromatic compounds (accounting for 24.2% total peak area). A small amount of esters (4, 3.0%), phenols (2, 2.4%), amide (1, 0.4%), and organic nitriles (1, 0.3%) were also identified. The carbon numbers of alkanes (except decane) ranged from 15 to 40, which are bio-refractory for conventional biological treatment. In addition, aromatic organic compounds and organic nitriles are toxic and refractory. This result may explain why the biodegradability of the raw wastewater (shown in Table 1) was very low.

Table 2 The main organic compounds identified in the secondary effluent with GC/MS.

Fig. 8. GC/MS chromatograms of: (a) raw wastewater, (b) treated by microbubble-ozonation, and (c) treated by macrobubble-ozonation.

By comparison, the chromatograms in Fig. 8b and 8c show that 14 and 10 organic contaminants were removed by microbubble-ozonation and macrobubble-ozonation, respectively, with the performance of the former being better than that of the latter. Furthermore, during microbubble-ozonation, four aromatic organic compounds, two phenols, one organic nitrile, and one amide were almost completely removed. The average relative removal efficiency of alkanes in microbubble-ozonation was 1.2 times higher than that in macrobubble-ozonation. The superior performance of microbubble-ozonation for the organic contaminant removal can be ascribed to the greater amount of the unselective hydroxyl radicals.

4. Conclusion

Microbubble-ozonation is a promising advanced oxidation process that can be applied for the treatment of refractory wet-spun acrylic fiber manufacturing wastewater. Microbubble-ozonation performed better than traditional macrobubble-ozonation for the degradation of bio-refractory organic compounds, with the higher removal efficiencies of COD_{cr}, NH_3-N, and UV_{254} of the wastewater being 25%, 9%, and 35% at the same ozone dose, due to its higher dissolution ability, longer ozone retention time, higher ozone utilization efficiency, faster ozone mass transfer coefficient, greater generation of hydroxyl radicals, and the relatively high surface zeta potential of microbubbles. The biodegradability of the wastewater was also highly improved by the microbubble-ozonation, which was ascribed to the enhanced degradation of alkanes, aromatic compounds, and many other bio-refractory organic compounds, as confirmed by gas chromatography/mass spectrometry (GC/MS).

Acknowledgments

The authors gratefully acknowledge the financial support of the Major Science and Technology Program for Water Pollution Control and Treatment (2012ZX07201002-6). Thanks also extend to Kikuchi ECO-Earth Co. Ltd. (Tokyo, Japan) for providing the microbubble generator and China Oil HBP Science & Technology Co., Ltd for providing the wastewater.

References

[1] H. Suty, C. De Traversay, M. Cost, Applications of advanced oxidation processes: present and future, Water Sci Technol, 49 (2004) 227-233.

[2] M. Khadhraoui, H. Trabelsi, M. Ksibi, S. Bouguerra, B. Elleuch, Discoloration and

detoxicification of a Congo red dye solution by means of ozone treatment for a possible water reuse, J Hazard Mater, 161 (2009) 974-981.

[3] J. Staehelin, J. Hoigne, Decomposition of ozone in water: rate of initiation by hydroxide ions and hydrogen peroxide, Environ Sci Technol, 16 (1982) 676-681.

[4] V. Camel, A. Bermond, The use of ozone and associated oxidation processes in drinking water treatment, Water Res, 32 (1998) 3208-3222.

[5] L.B. Chu, X.H. Xing, A.F. Yu, X.L. Sun, B. Jurcik, Enhanced treatment of practical textile wastewater by microbubble ozonation, Process Saf Environ, 86 (2008) 389-393.

[6] A. Agarwal, W.J. Ng, Y. Liu, Principle and applications of microbubble and nanobubble technology for water treatment, Chemosphere, 84 (2011) 1175-1180.

[7] M. Kukizaki, T. Wada, Effect of the membrane wettability on the size and size distribution of microbubbles formed from Shirasu-porous-glass (SPG) membranes, Colloids Surfaces A, 317 (2008) 146-154.

[8] U. Wattendorf, H.P. Merkle, PEGylation as a tool for the biomedical engineering of surface modified microparticles, J Pharm Sci-Us, 97 (2008) 4655-4669.

[9] P. Li, M. Takahashi, K. Chiba, Degradation of phenol by the collapse of microbubbles, Chemosphere, 75 (2009) 1371-1375.

[10] L.B. Chu, X.H. Xing, A.F. Yu, Y.N. Zhou, X.L. Sun, B. Jurcik, Enhanced ozonation of simulated dyestuff wastewater by microbubbles, Chemosphere, 68 (2007) 1854-1860.

[11] S. Liu, Q. Wang, T. Sun, C. Wu, Y. Shi, The effect of different types of micro-bubbles on the performance of the coagulation flotation process for coke waste-water, J Chem Technol Biot, (2012).

[12] F.S. Wei, W.Q. Qi, Z.G. Sun, Y.R. Huang, Y.W. Shen, Water and wastewater monitoring and analysis method, China Environmental Science Press, Beijing, (2002).

[13] R. Gehr, M. Wagner, P. Veerasubramanian, P. Payment, Disinfection efficiency of peracetic acid, UV and ozone after enhanced primary treatment of municipal wastewater, Water Res, 37 (2003) 4573-4586.

[14] W.A. APPA, Standard methods for the examination of water and wastewater, 21st Ed., American Public Health Association, American Water Work Association, Water Environment Federation, Washington, DC., 2005.

[15] J.M. Navaza, D. Gómez-Díaz, M.D. La Rubia, Removal process of CO< sub> 2 using MDEA aqueous solutions in a bubble column reactor, Chem Eng J, 146 (2009) 184-188.

[16] G.J. Price, E.J. Lenz, The use of dosimeters to measure radical production in aqueous sonochemical systems, Ultrasonics, 31 (1993) 451-456.

[17] M. Sahni, B.R. Locke, Quantification of hydroxyl radicals produced in aqueous phase pulsed electrical discharge reactors, Ind Eng Chem Res, 45 (2006) 5819-5825.

[18] R.W. Matthews, The radiation chemistry of the terephthalate dosimeter, Radiat Res, 83 (1980) 27-41.

[19] J.R. Baker, M.W. Milke, J.R. Mihelcic, Relationship between chemical and theoretical oxygen demand for specific classes of organic chemicals, Water Res, 33 (1999) 327-334.

[20] J. Hoigne, H. Bader, Ozonation of water: kinetics of oxidation of ammonia by ozone and hydroxyl radicals, Environ Sci Technol, 12 (1978) 79-84.

[21] S. Liu, Q. Wang, H. Ma, P. Huang, J. Li, T. Kikuchi, Effect of micro-bubbles on coagulation flotation process of dyeing wastewater, Sep Purif Technol, 71 (2010) 337-346.

[22] M. Takahashi, K. Chiba, P. Li, Free-radical generation from collapsing microbubbles in the absence of a dynamic stimulus, J Phys Chem B, 111 (2007) 1343-1347.

[23] M. Roustan, R.Y. Wang, D. Wolbert, Modeling hydrodynamics and mass transfer parameters in a continuous ozone bubble column, Ozone-Sci Eng, 18 (1996) 99-115.

[24] H. Zhou, D.W. Smith, Ozone mass transfer in water and wastewater treatment: experimental observations using a 2D laser particle dynamics analyzer, Water Res, 34 (2000) 909-921.

[25] P. Atkins, J. de Paula, Atkins' physical chemistry, Oxford University Press, 2014.

[26] P. Li, M. Takahashi, K. Chiba, Enhanced free-radical generation by shrinking microbubbles using a copper catalyst, Chemosphere, 77 (2009) 1157-1160.

[27] M. Takahashi, ζ potential of microbubbles in aqueous solutions: electrical properties of the gas-water interface, J Phys Chem B, 109 (2005) 21858-21864.

[28] C.D. DeMoyer, E.L. Schierholz, J.S. Gulliver, S.C. Wilhelms, Impact of bubble and free surface oxygen transfer on diffused aeration systems, Water Res, 37 (2003) 1890-1904.

[29] S. Liu, Q. Wang, X. Zhai, Q. Huang, P. Huang, Improved Pretreatment (Coagulation-Floatation and Ozonation) of Younger Landfill Leachate by Microbubbles, Water Environ Res, 82 (2010) 657-665.

[30] L.B. Chu, S.T. Yan, X.H. Xing, A.F. Yu, X.L. Sun, B. Jurcik, Enhanced sludge solubilization by microbubble ozonation, Chemosphere, 72 (2008) 205-212.

[31] S. Khuntia, S.K. Majumder, P. Ghosh, Removal of Ammonia from Water by Ozone Microbubbles, Ind Eng Chem Res, 52 (2012) 318-326.

[32] M. Takahashi, K. Chiba, P. Li, Formation of hydroxyl radicals by collapsing ozone microbubbles under strongly acidic conditions, J Phys Chem B, 111 (2007) 11443-11446.

[33] S. Usui, H. Sasaki, H. Matsukawa, The dependence of zeta potential on bubble size as determined by the dorn effect, J Colloid Interf Sci, 81 (1981) 80-84.

Table and Figures Legends

Table legends

Table 1 Characteristics of the acrylic fiber wastewater.

Table 2 The main organic compounds identified in the secondary effluent with GC/MS.

Figures legends

Fig. 1. Schematic diagram of the experimental setup.

Fig. 2. The variation of a) COD_{cr}, b) NH_3-N, c) UV_{254}, and d) BOD_5/COD_{cr} with time (solid symbols: microbubble-ozonation; open symbols: macrobubble-ozonation). Error bars represent standard deviation of three replicates.

Fig. 3. Gas holdup in deionized water during aeration with microbubble and macrobubble (solid symbols: microbubble-ozonation; open symbols: macrobubble-ozonation). Error bars represent standard deviation of three replicates.

Fig. 4. Dissolved ozone concentration (a) and ozone mass transfer coefficient (b) in deionized water of the two ozonation processes (solid symbols: microbubble-ozonation; open symbols: macrobubble-ozonation). Error bars in Fig. 4a represent standard deviation of three replicates.

Fig. 5. Ozone utilization efficiency and off-gas ozone concentration in the two ozonation processes (circle symbols: ozone utilization efficiency, angle symbols: off-gas concentration, solid symbols: microbubble-ozonation, and open symbols: macrobubble-ozonation).

Fig. 6. The fluorescence intensity of 2-hydroxyterephthalic acid (HTA) produced through the reaction of hydroxyl radicals with terephthalic acid (NaTA) in a) air- microbubble water, b) air-macrobubble water, c) ozone-microbubble water, and d) ozone-macrobubble water.

Fig. 7. pH variation with time during wastewater (a) and zeta potential of ozone microbubbles in deionized water at neutral and subalkalic condition (b) (solid symbols: microbubble-ozonation; open symbols: macrobubble-ozonation). Error bars in Fig. 7b represent standard deviation of three replicates.

Fig. 8. GC/MS chromatograms of: (a) raw wastewater, (b) treated by microbubble-ozonation, and (c) treated by macrobubble-ozonation.

Table 1 Characteristics of the acrylic fiber wastewater.

Parameter	COD_{cr} (mg/L)	BOD_5 (mg/L)	NH_3-N (mg/L)	TOC (mg/L)	UV_{254} (Abs/cm)	BOD_5/COD_{cr}	pH
Range of values	290-350	12-18	44-69	80-150	0.30-0.45	0.035-0.05	6.5-8.3
Average value ± S.D.	326 ± 29	14 ± 2	67 ± 9	116 ± 23	0.40 ± 0.05	0.04 ± 0.01	8.0 ± 0.3

Note: S.D. is abbreviation of standard deviation.

Table 2 The main organic compounds identified in the secondary effluent with GC/MS.

No	Retention time (min)	Chemicals	Similarity (%)	Area (Mean ± S.D.)	a* (%) (Mean ± S.D.)	b* (%) (Mean ± S.D.)
1	7.492	Toluene	92	96268 ± 2066	85.9 ± 1.9	78.9 ± 1.7
2	9.783	Ethyl-benzene	90	56005 ± 1210	84.9 ± 2.1	75.6 ± 1.6
3	10.000	1,2-dimethyl-Benzene	88	88187 ± 1815	91.0 ± 2.5	82.3 ± 1.9
4	10.508	Ethenyl-benzene	90	764446 ± 18128	100 ± 0.0	95.3 ± 2.0
5	11.142	N,N-dimethylacetamide	81	13300 ± 345	100 ± 0.0	99.0 ± 1.0
6	12.083	Benzenol	93	47738 ± 1134	89.5 ± 2.1	76.1 ± 1.9
7	12.642	Decane	95	45274 ± 772	42.6 ± 1.0	15.2 ± 0.4
8	13.742	Sulfurous acid, hexyl octyl ester	86	46652 ± 1212	65.8 ± 1.5	48.5 ± 1.2
9	13.950	2-methyleneglutaronitrile	92	19616 ± 421	65.8 ± 1.7	10.4 ± 0.2
10	14.592	4,6-dimethyl-Dodecane	89	21626 ± 467	47.5 ± 1.1	19.5 ± 0.4
11	15.133	Pentanedioic acid, dimethyl ester	89	15336 ± 384	57.0 ± 1.5	39.1 ± 0.9
12	15.733	2-phenyl-Tridecane	84	122701 ± 2801	83.3 ± 1.8	50.5 ± 1.1
13	16.367	Pentadecane	96	220794 ± 3763	49.2 ± 1.3	20.4 ± 0.4
14	16.742	Oxalic acid, 4-chlorophenyl octyl ester	82	34611 ± 959	89.3 ± 2.2	69.9 ± 1.8
15	16.983	Adipic acid, ethyl methyl ester	85	45739 ± 1003	62.9 ± 1.3	55.0 ± 1.3
16	18.375	Heneicosane	96	34784 ± 887	56.1 ± 1.6	26.9 ± 0.6
17	18.717	Heptadecane	96	210182 ± 4895	51.0 ± 1.2	26.1 ± 0.7
18	19.567	Hexadecane	96	174163 ± 3326	48.8 ± 1.1	23.1 ± 0.6
19	20.900	Eicosane	97	69921 ± 1817	54.3 ± 1.2	29.0 ± 0.7
20	21.242	2,4-Di-tert-butylphenol	91	64842 ± 1392	86.4 ± 2.3	80.5 ± 1.8
21	22.383	Heneicosane	97	77306 ± 1904	56.0 ± 1.3	29.5 ± 0.6
22	23.333	Pentacosane	97	728050 ± 17295	60.8 ± 1.6	21.1 ± 0.5
23	23.800	Dotriacontane	98	646208 ± 11343	62.4 ± 1.4	30.1 ± 0.6
24	25.175	Heneicosane	99	131711 ± 3534	55.2 ± 1.4	27.4 ± 0.5
25	25.300	Tetracosane	97	108228 ± 2323	60.1 ± 1.5	24.6 ± 0.6
26	26.925	Hexatriacontane	98	169633 ± 4475	64.0 ± 1.3	26.2 ± 0.6
27	27.117	Tetracontane	96	614965 ± 13754	65.8 ± 1.8	27.2 ± 0.6

Note: a*: relative removal efficiency in microbubble-ozonation, b*: relative removal efficiency in macrobubble-ozonation.

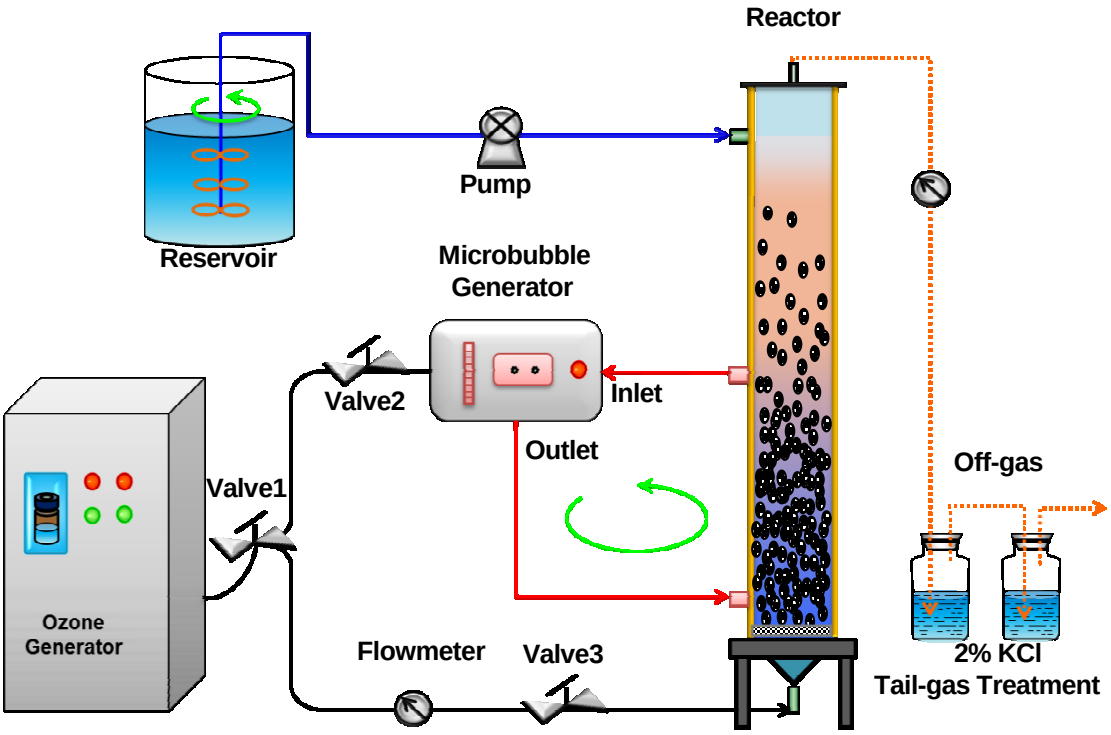

Fig. 1. Schematic diagram of the experimental setup.

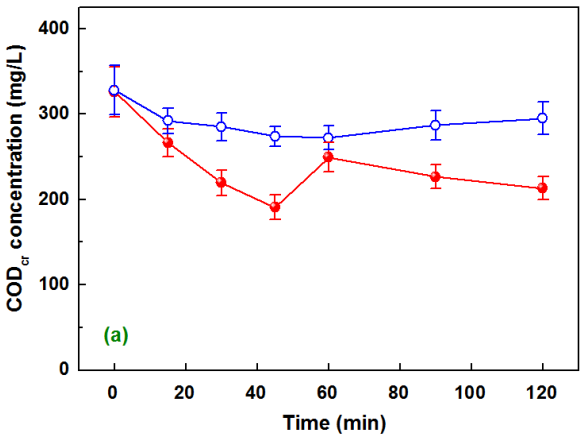

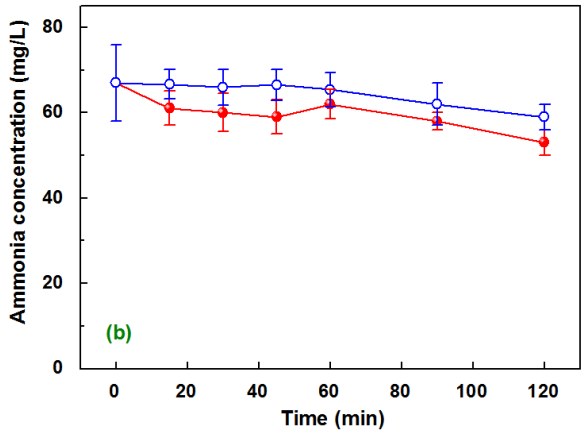

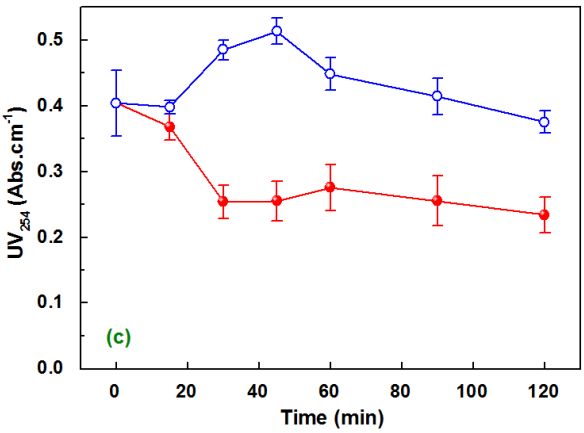

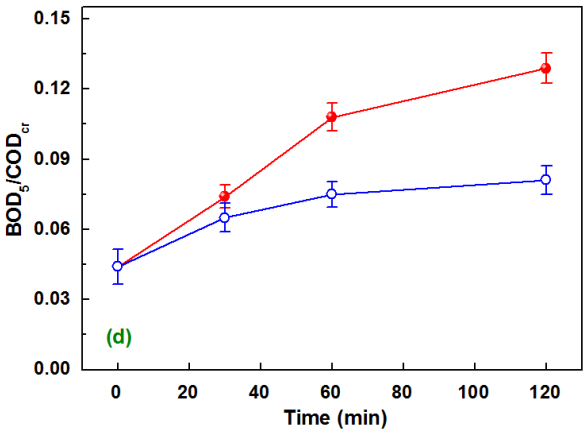

Fig. 2. The variation of a) COD_{cr}, b) NH_3-N, c) UV_{254}, and d) BOD_5/COD_{cr} with time (solid symbols: microbubble-ozonation; open symbols: macrobubble-ozonation). Error bars represent standard deviation of three replicates.

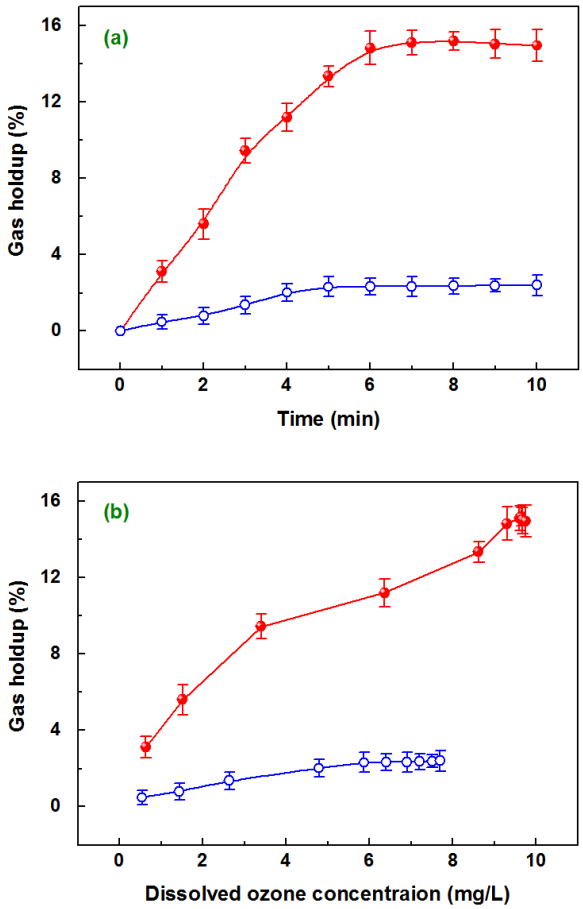

Fig. 3. Gas holdup in deionized water during aeration with microbubble and macrobubble (solid symbols: microbubble-ozonation; open symbols: macrobubble-ozonation). Error bars represent standard deviation of three replicates.

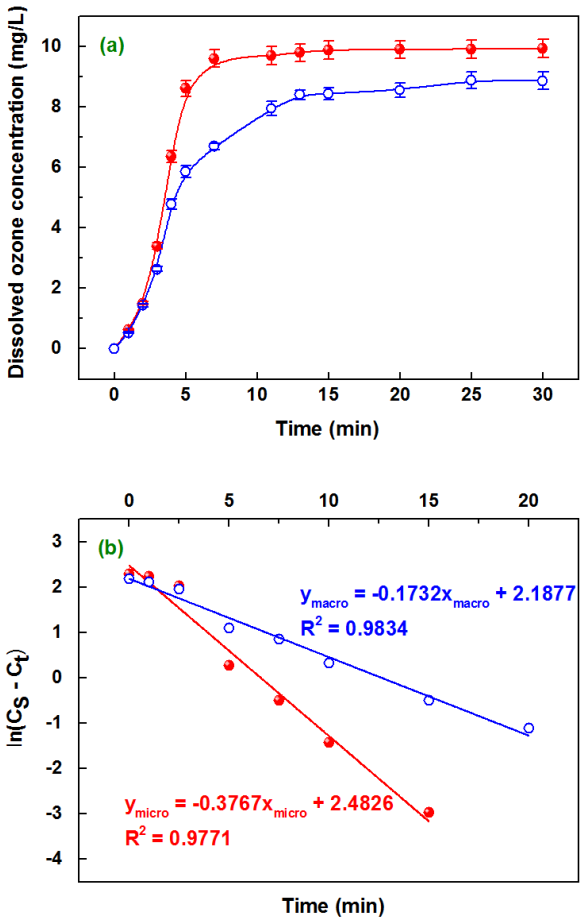

Fig. 4. Dissolved ozone concentration (a) and ozone mass transfer coefficient (b) in deionized water of the two ozonation processes (solid symbols: microbubble-ozonation; open symbols: macrobubble-ozonation). Error bars represent standard deviation in Fig. 4a.

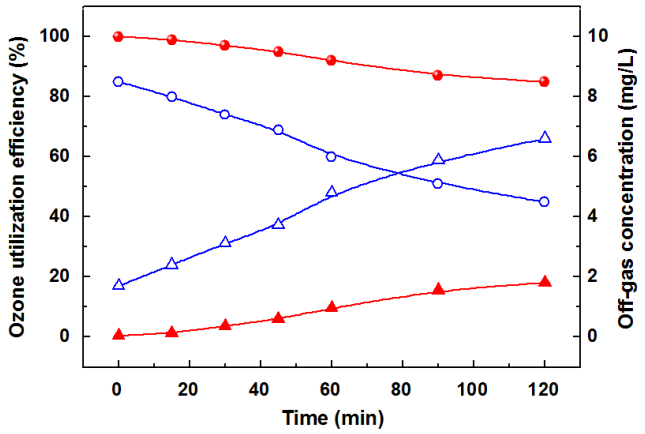

Fig. 5. Ozone utilization efficiency and off-gas ozone concentration in the two ozonation processes (circle symbols: ozone utilization efficiency, angle symbols: off-gas concentration, solid symbols: microbubble-ozonation, and open symbols: macrobubble-ozonation).

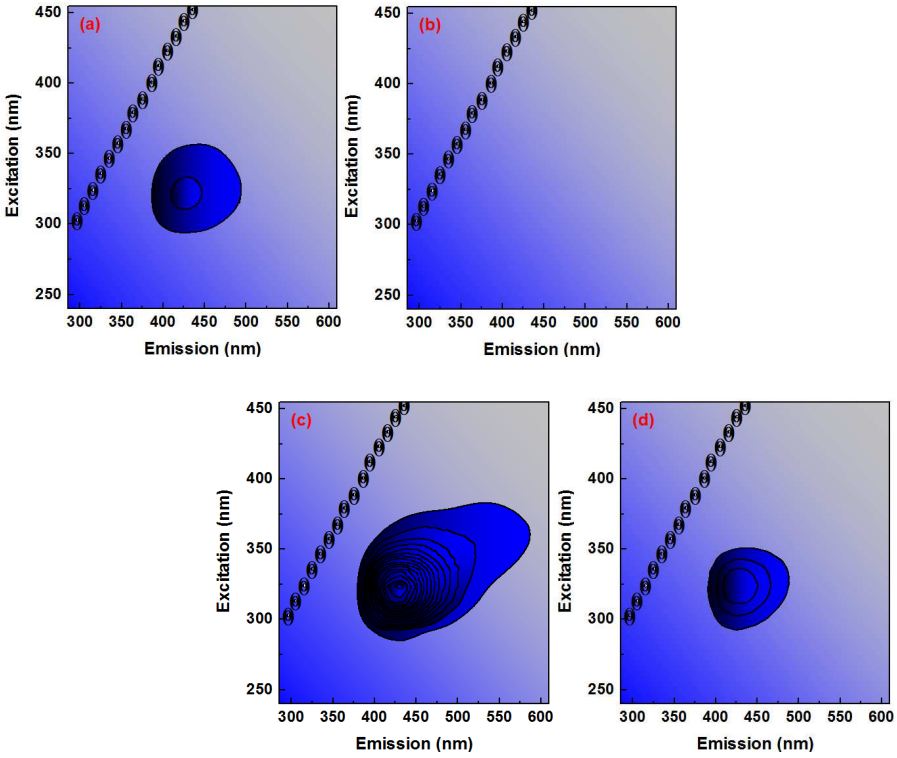

Fig. 6. The fluorescence intensity of 2-hydroxyterephthalic acid (HTA) produced through the reaction of hydroxyl radicals with terephthalic acid (NaTA) in a) air- microbubble water, b) air-macrobubble water, c) ozone-microbubble water, and d) ozone-macrobubble water.

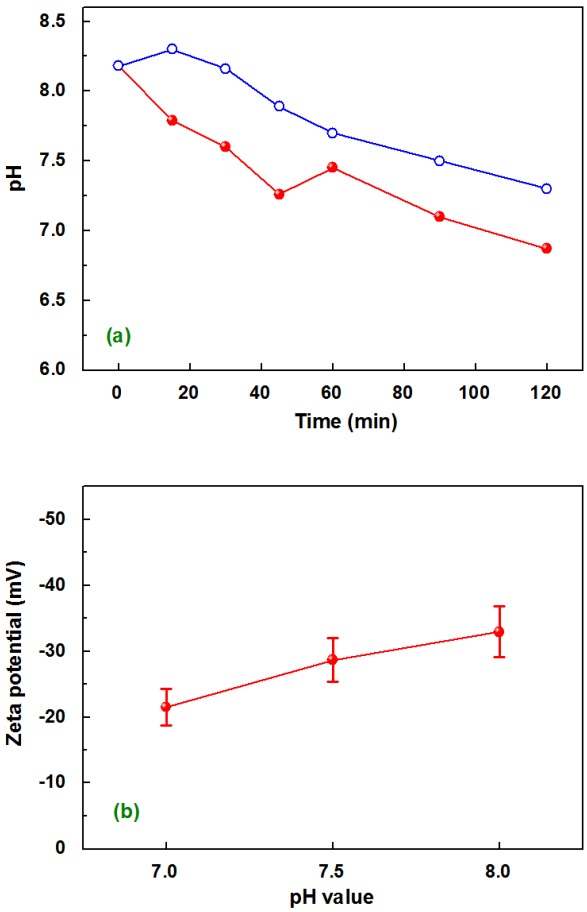

Fig. 7. pH variation with time during wastewater (a) and zeta potential of ozone microbubbles in deionized water at neutral and subalkalic condition (b) (solid symbols: microbubble-ozonation; open symbols: macrobubble-ozonation). Error bars in Fig. 7b represent standard deviation of three replicates.

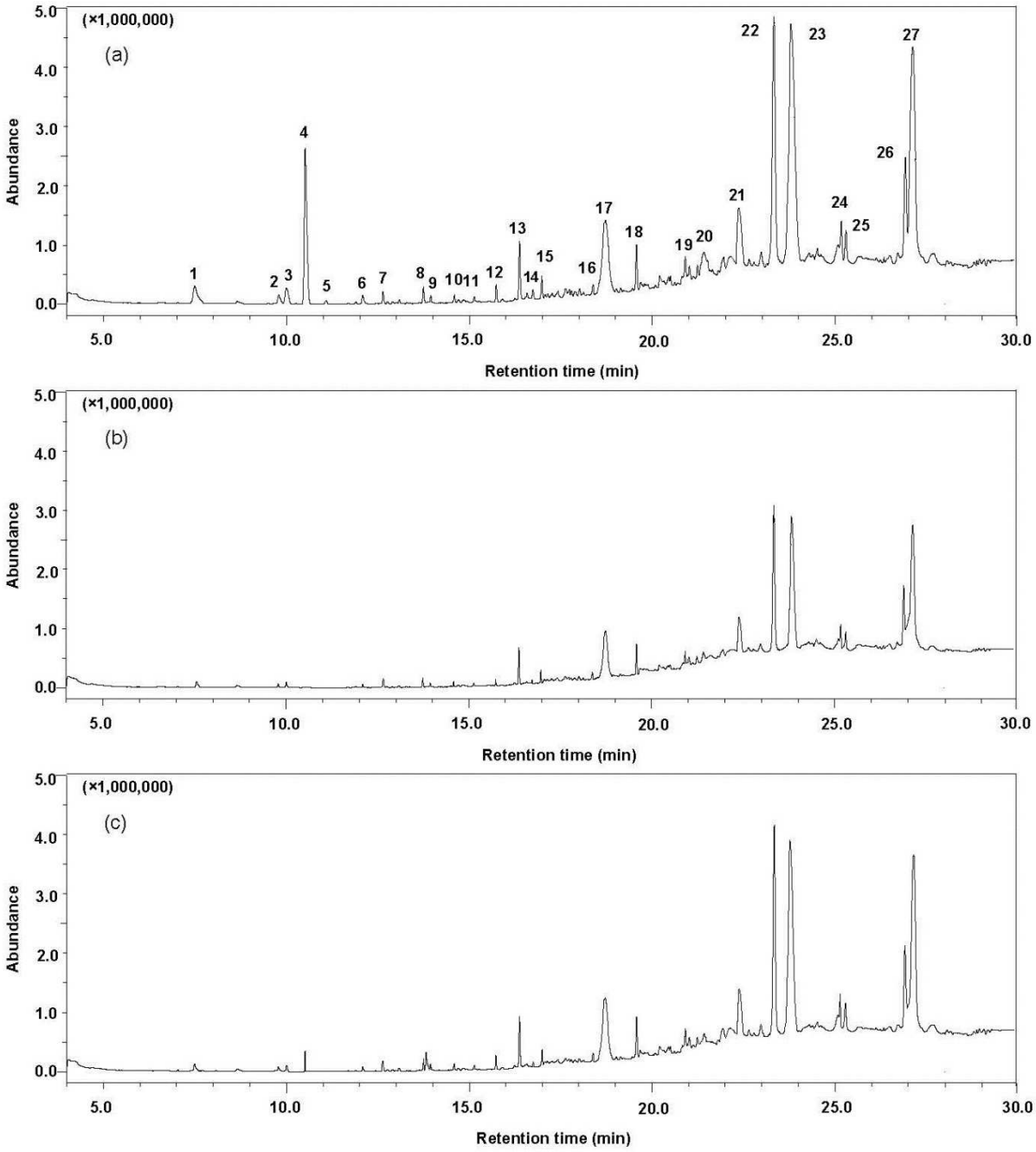

Fig. 8. GC/MS chromatograms of: (a) raw wastewater, (b) treated by microbubble-ozonation, and (c) treated by macrobubble-ozonation.